Blood flow coordinates collective endothelial cell migration during vascular plexus formation and promotes angiogenic sprout regression via *vegfr3/flt4*

Yan Chen[1], Aaron M. Savage[2] Zhen Jiang[3, 4], Hyejeong R. Kim [5], Paul C. Evans[6]* and Robert N. Wilkinson[2]*

1 Department of Infection, Immunity and Cardiovascular Disease, University of Sheffield, UK
2 School of Life Sciences, Medical School, University of Nottingham, UK
3 Max Planck Institute for Heart and Lung Research, Department of Developmental Genetics, Bad Nauheim 61231, Germany.
4 German Centre for Cardiovascular Research (DZHK), Partner Site Rhine-Main, Bad Nauheim 61231, Germany.
5 Department of Biomedical Science, University of Sheffield, UK
6 William Harvey Research Institute, Queen Mary University of London, UK

*Equal contribution

Author for correspondence
Robert Wilkinson
rob.wilkinson@nottingham.ac.uk
Phone: +44 115 823 1429

Abstract

Nascent vascular networks adapt to the increasing metabolic demands of growing tissues by expanding via angiogenesis. As vascular networks expand, blood vessels remodel, progressively refining vascular connectivity to generate a more haemodynamically efficient network. This process is driven by interplay between endothelial cell (EC) signalling and blood flow. While much is known about angiogenesis, considerably less is understood of the mechanisms underlying vessel remodelling by blood flow. Here we employ the zebrafish sub-intestinal venous plexus (SIVP) to characterise the mechanisms underlying blood flow-dependent remodelling. Using live imaging to track ECs we show that blood flow controls SIVP remodelling by coordinating collective migration of ECs within the developing plexus. Blood flow opposes continuous ventral EC migration within the SIVP and is required for regression of angiogenic sprouts to support plexus growth. Sprout regression occurs by coordinated polarisation and migration of ECs from non-perfused leading sprouts, which migrate in opposition to blood flow and incorporate into the SIV. Sprout regression is compatible with low blood flow and is dependent upon *vegfr3/flt4* function under these conditions. Collectively, these studies reveal how blood flow sculpts a

developing vascular plexus by coordinating EC migration and balancing vascular remodelling via *vegfr3/flt4*.

Introduction

During early development, cellular uptake of nutrients and elimination of metabolic waste must occur prior to the formation of specialised organs responsible for these functions. Consequently, the nascent vascular networks that mediate metabolic exchange must undergo rapid adaptation to accommodate the dynamic metabolic demands of growing tissues. As vascular networks expand, they must optimise metabolic exchange while minimising resistance to blood flow. Evolution has therefore favoured mechanisms that enhance haemodynamic efficiency (Campinho et al., 2020). Angiogenic sprouting must be balanced with vascular remodelling to maintain haemodynamic efficiency during network expansion. Remodelling occurs either by fusion or regression of angiogenic sprouts to form functional tubular vessels, or the pruning of redundant blood vessels (Ribatti and Crivellato, 2012). Endothelial cells (ECs), which line the inner surface of blood vessels play a central role in this process by responding dynamically to changes in their local environment (Udan et al., 2013). While most blood vessels develop from pre-existing patent vessels with stable blood flow, our understanding of the mechanisms governing vascular remodelling and the influence of blood flow on these processes remains incomplete. For example, it is not yet clear whether vascular regression is driven by active signalling pathways, the withdrawal of survival cues, or a combination of both, nor whether these mechanisms vary across vascular beds (Korn and Augustin, 2015).

The vascular network of the zebrafish sub-intestinal venous plexus (SIVP) forms bilaterally in the embryo and is structurally similar to the mammalian vitelline veins which connect the embryo with extraembryonic circulation in the yolk sac (Goi and Childs, 2016). Owing to its developmental plasticity the SIVP has become a valuable model for investigating the cellular mechanisms underlying vascular remodelling (Goi and Childs, 2016; Hen et al., 2015; Koenig et al., 2016; Lenard et al., 2015). The SIVP initially facilitates nutrient uptake from the yolk and later contributes to vascularisation of the larval the digestive system (Isogai et al., 2001). The SIVP comprises the supra-intestinal artery (SIA), bilateral sub-intestinal veins (SIV) and inter-connecting vessels (ICVs) which connect the SIA and SIV (Fig. 1A). The SIVP originates from angioblasts in the ventral posterior cardinal vein, which give rise to both the SIA and the SIV (Goi and Childs, 2016; Hen et al., 2015; Koenig et al., 2016). The primitive SIVP expands bilaterally over the yolk surface and ECs from the primary SIV migrate dorsally throughout the plexus to form branches and the SIA (Goi and Childs, 2016; Hen et al., 2015; Koenig et al., 2016). In mammals, progressive refinement of a vascular network by vessel pruning or regression involves dynamic migration and rearrangement of ECs (Franco et al., 2016, 2015; Udan et al., 2013). ECs are capable of migrating within patent blood vessels during vascular network formation (Christ et al., 1990;

Franco et al., 2015) leading us to hypothesise that coordinated EC motility is essential for SIVP remodelling and may be regulated by blood flow.

Vascular Endothelial Growth Factor (VEGF) signalling controls diverse aspects of EC biology, including migration and survival (Akeson et al., 2010; Ferrara et al., 2003). VEGF ligands signal via their cognate receptor tyrosine kinase receptors VEGFR1-3, with VEGFR2 serving as the principal signalling receptor in mammalian blood ECs (Simons et al., 2016). In zebrafish, Vegfr4/Kdrl and Vegfr2/Kdr are functionally analogous to mammalian VEGFR2 (Bussmann et al., 2008). ECs sense blood flow via junctional mechanosensory complexes, most notably the VE-cadherin, PECAM-1, VEGFR2/3 complex, which operates independently of VEGF ligands and is essential for arterial vascular remodelling (Coon et al., 2015; Tzima et al., 2005). Endothelial VEGFR3/Flt4 levels establish a fluid shear stress set point, and sustained deviations from this threshold trigger vascular remodelling in arteries (Baeyens et al., 2015; Tzima et al., 2005). Zebrafish *vegfaa* mutants exhibit severe defects in SIVP formation (Habeck et al., 2002; Koenig et al., 2016) and combined loss of *kdr* and *kdrl* similarly disrupts SIVP development (Habeck et al., 2002; Koenig et al., 2016). Sprout pathfinding within the SIVP depends on the guidance receptor, PlexinD1, and plexus expansion is constrained by inhibition of Bone Morphogenetic Protein (BMP) signalling (Goi and Childs, 2016). SIVP remodelling occurs via flow-dependent pruning and fusion of vessel branches (Hen et al., 2015; Lenard et al., 2015). Retraction of SIVP leading sprouts has been observed (Hen et al., 2015), but whether this process is flow-dependent remains unknown. Moreover, a systematic analysis of EC migration during SIVP formation is lacking and the interplay between blood flow and signalling pathways in co-ordinating plexus remodelling remains poorly understood.

Here we demonstrate that blood flow plays a critical role in coordinating EC migration during vascular plexus formation and remodelling. Through time-lapse imaging and quantitative analysis, we show that blood flow orchestrates collective EC migration throughout the developing SIVP and promotes regression of leading angiogenic sprouts to support plexus expansion. Our data suggest that sprout regression occurs by coordinated EC rearrangement between non-perfused sprouts and the vessel lumen, driven by directed EC polarisation and migration against blood flow. Using erythrocyte depletion to reduce circulation, we find that sprout regression can occur under low flow conditions, but this process requires *flt4* function. Together, these findings provide a clear view of the complex cellular dynamics underlying vessel remodelling during vascular plexus formation and highlight the central role of EC responses to blood flow.

Methods

Zebrafish strains

108 Maintenance of zebrafish and experimental procedures involving zebrafish were carried out according
109 to UK national guidelines and under UK Home Office licenses. The following zebrafish lines were
110 employed in this study: *Tg(fli1a:*EGFP*)*^{y1} (Lawson and Weinstein, 2002)*, Tg(gata1a:*DsRed*)*^{sD2} (Traver
111 et al., 2003), *Tg(fli1a:AC-TagRFP)*^{SH511}(Savage et al., 2019), *Tg(kdrl:EGFP)*^{s843} (Jin et al., 2005),
112 *Tg(fli1a:nls*-mCherry*)*^{SH550} (this study), *Tg(fli1a:nls*-EGFP*)*^{SH549} (this study), *Tg(fli1a:golgi*-TagRFP*;*
113 *cryaa:*CFP*)*^{SH529} (this study), *flt1*^{bns29} (Matsuoka et al., 2016), *flt4*^{qmc316}, (this study).
114
115 **Generation of Transgenic lines**
116 *Tg(fli1a:nls*-EGFP*)*^{SH549} and *Tg(fli1a:nls-mCherry)*^{SH550} were generated using the Tol2 Kit (Kwan et al.,
117 2007) via standard methods as previously described (Savage et al., 2019) using the following
118 components: p5E-fli1aep (Villefranc et al., 2007) pME-mCherry or pME-EGFP, p3E-SV40pA, and
119 pDestTol2-pA2. *Tg(fli1a:golgi-TagRFP, cryaa:cerulean)*^{SH529} was generated by fusing amino acids 1-60
120 of Human B4GALT1 to the N-terminus of TagRFP via *in silico* synthesis. attB1/attB2R sites were added
121 to the fusion product by PCR (Supplementary Table 1) to generate pME-Golgi-TagRFP. The *fli1a:golgi*-
122 TagRFP*; cryaa:*CFP construct was generated using the Tol2 Kit and the following components: p5E-
123 fli1aep, pME-Golgi-TagRFP, p3E-SV40pA, and pDestTol2cryCFP. Embryos were injected at one-cell
124 stage with 25 ng/µl *Tol2* mRNA and corresponding plasmid DNA.
125
126 **Microinjection of morpholinos and mRNA**
127 Microinjections were performed on single cell embryos with 1nl injection volume. Embryos were injected
128 with 0.8ng morpholinos (Supplementary Table 1) including control, *tnnt2a* (Sehnert et al., 2002), *flt4*
129 (Hogan et al., 2009b), and *gata1a* (Galloway et al., 2005) or 200pg mRNA including *mTurquoise2* and
130 $vegfaa_{165}$ (Lawson et al., 2002).
131
132 **G0 *tnnt2a* CRISPR mutants**
133 Target sequences were ordered as crRNAs (Merck) based on previously published sequences (Wu et
134 al., 2018) (Supplementary Table 1) and co-injected alongside tracrRNA (Merck) in equimolar ratios and
135 EnGen®Spy Cas9 NLS protein (NEB) into 1-cell zebrafish embryos.
136
137 **RNA *in situ* hybridisation**
138 Alkaline phosphatase wholemount *in situ* hybridisation experiments were performed using standard
139 methods as described previously (Wilkinson et al., 2012) using probes against *mflt1* (Krueger et al.,
140 2011), *sflt1* (Krueger et al., 2011), *flt4* (Thompson et al., 1998), *kdrl* (Fouquet et al., 1997). Detailed
141 protocols are available upon request.
142
143 **Live imaging of zebrafish embryos and larvae**

144 Zebrafish were anaesthetised using Tricaine (MS-222, Sigma-Aldrich) and embedded in 1% low-
145 melting point agarose which was held in place in a glass capillary and imaged using a light sheet Z.1
146 microscope (Zeiss), or Cell Discoverer 7 microscope (Zeiss). The chamber contained E3 and tricaine
147 (164mg/L) to ensure embryos and larvae remained anaesthetised throughout imaging. Imaging was
148 performed at 28.5°C. Images were acquired using ZEN software (Zeiss). Zebrafish were imaged at 5-
149 minute intervals to detect blood flow, and 10-minute intervals to track EC nuclei. To image individual
150 erythrocytes in *gata1a* morphants, time lapses were taken at 50 frames per second for 30 seconds with
151 1 µm z-stacks. The number of erythrocytes which passed a defined region of the SIV within a 30 second
152 period were manually counted.
153
154 **Quantification of SIVP morphology**
155 Image quantification and analysis was performed using FIJI (Schindelin et al., 2012). Parameters
156 employed to quantify SIVP morphology including area, length, vascular loops, sprout number and EC
157 number, were recorded in a region of 5 somite widths. The length of the SIVP was measured as the
158 vertical distance from the SIA to the most ventral part of the SIV. To ensure only endothelial nuclei
159 within the SIVP were quantified, dual channel fluorescence was employed to highlight EC cytosol and
160 nuclei. To quantify average SIV diameter, the SIV was measured at three equidistant points positioned
161 anteroposteriorly and mean value was calculated.
162
163 **EC rearrangement and cell trajectory analysis**
164 *Tg(fli1a:nls*-mCherry*)*^{SH550} heterozygous embryos were used for cell tracking studies. Time-lapse
165 images were pre-processed using Linear Stack Alignment with SIFT (Lowe, 2004) in FIJI and the
166 movements of EC nuclei were tracked using TrackMate (Tinevez et al., 2017). Any misconnected tracks
167 were manually corrected. Tracking data was exported and analysed using customised MATLAB scripts
168 freely available at https://github.com/yanc0913/SIVP_cell_tracking (Chen et al., 2022). ECs were colour
169 coded as tip cells (magenta), SIVP branches (orange), or SIV cells (blue) depending upon their initial
170 position at the start of tracking (56 hours post fertilisation, hpf). At the end of observation (72 hpf), cell
171 positions were evaluated to determine whether ECs moved between EC subsets e.g., an EC initially
172 located in the SIV which migrated to a branch by the end of tracking was recorded as a single
173 rearrangement event. The number of ECs at initial and final position and the events of EC
174 rearrangement were manually recorded from each time lapse. To analyse migration trajectory, a
175 migration step was defined as one cell at position 1 (x_1 and y_1) migrating to its subsequent position 2
176 (x_2 and y_2) in a time range (from t_1 to t_2). The distance (or displacement) of the step (or the track) was
177 calculated as . Track distance was the sum of step displacements. Migration velocity was calculated as
178 step displacement divided by time interval, and the mean velocity at a particular time range was the
179 average of each velocity in that range. The angle of each migration step was calculated using the four-
180 quadrant inverse tangent (*atan2)* function in MATLAB, which computed the arctangent of Δy and Δx.

181

182 **Quantification of EC Golgi polarity**

183 In sprout cells, the position of the Golgi at either dorsal (45-135°) or ventral (225-315°) end of the
184 elongated EC nucleus was considered polarised. In SIV cells, the position of the Golgi at either anterior
185 (or downstream of blood flow, 135-180°) or posterior (or upstream of blood flow, 0-45°) end of the
186 elongated EC nucleus was considered polarised.

187

188 **Generation of *flt4*^{qmc316} allele**

189 gRNAs targeting *flt4* (ENSDARG00000104453) were ordered from IDT DNA Technologies and targeted
190 the following sequence 5'-CCCAGGGTATAGAGAAATCAGGC-3' in exon 3. crRNAs were annealed
191 with tracrRNA (IDT) as previously described (Kroll et al., 2021). Annealed sgRNAs were injected into
192 1-cell stage zebrafish embryos alongside EnGen® Spy Cas9 NLS (NEB #M0646) in a non-complexed
193 solution. F1 progeny of G0 embryos were genotyped using high resolution melt analysis and PCR using
194 the following primers 5'- AGTGGAGTTTACTGATCGCCA-3', 5'- CCGTGGTGCCATCAATAACA-3' to
195 confirm the presence of the *flt4*^{qmc316} allele. *flt4*^{qmc31} consists of a complex insertion and deletion resulting
196 in a net 132bp insertion, which is predicted to shift frame after 83 residues and truncate following 11
197 subsequent incorrect residues within the first extracellular Ig-like domain and earlier than previously
198 published *flt4* alleles including a reported null allele within exon 4 (Shin et al., 2016).

199

200 **Statistical analyses**

201 Statistical analyses and graph plots were performed using GraphPad Prism. All statistical analysis is
202 described in figure legends, including paired/unpaired *t*-test, ordinary one-way ANOVA, and two-way
203 ANOVA. All error bars display the mean and standard deviation in the figures. *p*-values, unless exact
204 value is listed, are as follows: ns= not significant, *=<0.05, **=≤0.01, ***=≤0.001, ****=≤0.0001.

205

206 **Results**

207 **Blood flow controls SIVP remodelling by influencing EC distribution and promoting**
208 **leading sprout regression.**

209 The SIVP develops from angiogenic sprouts which emerge from the posterior cardinal vein (PCV) by
210 30 hpf and migrate in a ventrolateral direction, bilaterally, over the surface of the yolk (Goi and Childs,
211 2016; Hen et al., 2015; Koenig et al., 2016). To determine the timing of SIVP development in relation
212 to blood flow, we imaged the developing plexus in the presence of fluorescently labelled erythrocytes
213 (Fig.1A). Between 53 hpf and 55 hpf, blood flow entered the nascent SIVP anteriorly via the supra-
214 intestinal artery (SIA) (Fig. 1A-C"). Circulation progressed from anterior to posterior, and by 72 hpf the
215 plexus became fully perfused (Fig. 1D-F", G supplementary movie 1). As the SIVP becomes perfused,
216 it undergoes extensive remodelling. Migrating angiogenic sprouts, hereafter referred to as leading

217 sprouts, protrude from the ventral sub intestinal vein (SIV) and were observed to either fuse with
218 neighbouring sprouts or regress, with their ECs reintegrating into the SIV by 70 hpf (Fig. 1H-J, arrows,
219 supplementary movie 1 and 2, arrowheads).
220
221 Remodelling of leading sprouts coincided with the onset of blood flow in the SIV. After flow began, new
222 leading sprouts were rarely formed in the SIVP, and most existing sprouts underwent regression.
223 Therefore, we defined the period following flow onset as the sprout regression phase. To determine
224 whether this process depends on blood flow, we inhibited cardiac contraction and circulation using a
225 morpholino targeting cardiac troponin T type 2a (*tnnt2a*) and examined SIVP morphology (Fig. 2).
226 Although the overall size of the SIVP was unchanged in *tnnt2a* morphants compared to controls, (Fig.
227 2A-B', C), its morphology was altered (Fig. 2A, B). Specifically, morphants exhibited fewer vascular
228 loops (Fig.2A', B' asterisks, D), reduced dorsoventral plexus length (Fig. 1A', B', E) and increased length
229 (Fig. 2A', B', E) and number of leading sprouts (Fig. 2A", B", E, F). While the total EC number of the
230 SIVP was not significantly different between morphants and controls (Fig. 2G), EC distribution was
231 affected (Fig. 2A", B", H, I). Leading sprouts in morphants contained more ECs (Fig. 2A", B", H, I),
232 whereas SIVP branches had significantly fewer. However, EC numbers in the ventral region of the SIVP
233 (the sub intestinal vein, SIV), were not significantly altered (Fig. 2A", B", I).
234
235 To control for potential off target effects induced by morpholino injection, we generated G0 *tnnt2a*
236 CRISPR mutants (Wu et al., 2018) and assessed SIVP morphology. Mosaic *tnnt2a* mutants displayed
237 abnormal plexus morphology (Fig. S1A, B arrows, C-I), phenocopying the defects observed in
238 morphants (Fig. 2), confirming that these changes were specific to *tnnt2a* inhibition.
239
240 Together, these findings suggest that blood flow influences EC distribution within the developing venous
241 plexus without affecting the total EC number. The increased size and frequency of leading sprouts in
242 *tnnt2a* morphants further suggest that blood flow promotes sprout regression. Consistent with this,
243 leading sprouts regressed in the presence of flow, with their ECs integrating into the SIV (Fig. 3A-C,
244 arrows, Supplementary Movie 3). In contrast, sprout regression was significantly reduced in *tnnt2a*
245 morphants which retained more leading sprouts by 72 hpf. Anastomosis of leading sprouts was rare
246 and occurred independently of blood flow (Fig. 3A, asterisk, G, H, Supplementary movie 3). Overall,
247 these data indicate that blood flow contributes to SIVP remodelling, in part by promoting regression of
248 leading sprouts.
249
250 **Blood flow controls EC migration but not proliferation within the developing SIVP**
251 The distribution of ECs within the developing SIVP could be influenced by several factors, including
252 differences in cell proliferation, apoptosis, or migration. Although the total number of ECs within the

253 SIVP remained unchanged in the absence of blood flow (Fig. 2G), the altered spatial distribution of ECs
254 (Fig. 2H, I) suggested that flow might affect local rates of proliferation or apoptosis across. To
255 investigate whether differences in EC proliferation, apoptosis, or migration contributed to the altered
256 EC distribution observed in plexuses formed without blood flow (Fig. 2I), we tracked EC behaviour in
257 the developing SIVP of control embryos and *tnnt2a* morphants between 56 and 70 hpf (Fig. 4,
258 Supplementary Movie 4, 5). Similar numbers of ECs were tracked at the beginning of each time-lapse
259 and ECs were grouped by their location at 56hpf, either within SIVP branches, SIV, or tip cells within
260 leading sprouts (Fig. 4A-B). Endothelial proliferation was unaffected by the flow status of the developing
261 plexus (Fig. 4C), and no apoptotic events were observed during SIVP development in either the
262 presence or absence of blood flow. Thus, differential proliferation or apoptosis were unlikely to account
263 for altered EC distribution observed in *tnnt2a* morphants (Fig. 2I). However, in the absence of blood
264 flow, the frequency with which ECs differentially contributed to neighbouring EC subsets was altered
265 (Fig. 4D). In the presence of blood flow, 73% of leading sprouts consisted of a pair of endothelial tip
266 cells positioned in parallel to each other, which is consistent with previous reports (Hen et al., 2015).
267 When tip cells divided in the presence of blood flow (Fig. 4B), the dorsal daughter cell rapidly migrated
268 dorsally in most cases (77%), to contribute to the SIV (Supplementary Movie 6, arrows). This left the
269 paired tip cells within the sprout, suggesting that the migrating daughter cell adopted a stalk identity
270 (Supplementary Table 2). In rare cases (<2%) with blood flow present, daughter cells that migrated
271 dorsally from leading sprouts to the SIV were later observed contributing to SIVP branches by 72 hpf
272 (Fig. 4D). ECs were not seen migrating into leading sprouts under normal flow conditions. However,
273 occasional bending and transient repositioning of EC nuclei at the boundary between the SIV and
274 leading sprouts were observed, suggesting limited plasticity at this interface. In contrast, in the absence
275 of blood flow, only 25% of tip cells migrated dorsally to the SIV, with most tip cells remaining within the
276 leading sprout by 72 hpf. This aligns with the increased numbers of ECs observed in leading sprouts of
277 *tnnt2a* morphants (Fig. 2B", I, S1I). Notably, in *tnnt2a* morphants, SIV ECs were seen migrating ventrally
278 into leading sprouts (Fig. 4D). Interestingly, these migrating ECs did not appear to compete with tip
279 cells at the sprout front, suggesting they did not acquire tip cell identity.
280
281 ECs within SIVP branches make up approximately half of the total EC population within the plexus, yet
282 they rarely change position in the presence of blood flow. Fewer than 1% of ECs in branches contributed
283 to cellular rearrangement during SIVP development (Supplementary Table 2, Fig. 4D). In contrast, ECs
284 from branches were significantly more likely to migrate into the SIV in *tnnt2a* morphants (Fig. 4D).
285 Although the overall number of EC positional changes was not significantly different between control
286 and *tnnt2a* morphants (Figure 4D), the direction of migration varied. ECs tended to migrate dorsally in
287 the presence of flow, while ventral migration was more common in plexuses that developed without
288 flow, resulting in an increased tendency for ECs to adopt and maintain tip cell behaviour (Fig. 4D).

289 Collectively, these data suggest that blood flow is required to guide the directional rearrangement of
290 ECs during SIVP development.
291
292 In the presence of blood flow, ECs within the SIVP exhibited distinct migratory behaviours depending
293 upon their location. While the plexus expanded and ECs migrated ventrally, blood flow promoted dorsal
294 migration, likely supporting coordinated plexus growth (Fig. 4E). In the absence of blood flow, ECs
295 showed persistent ventral movement, leading to distended SIVP branches with fewer cells (Fig. 3C, F)
296 and elongated leading sprouts with accumulated ECs displaying tip cell behaviour (Fig. 4E).
297

298 **Blood flow co-ordinates the direction of EC migration during SIVP development**

299 During SIVP remodelling, ECs displayed distinct migratory behaviours depending upon their position
300 within the plexus and the presence or absence of blood flow (Fig. 4D). To investigate whether blood
301 flow influences EC migration, we focused on the most ventral ECs within each SIVP, particularly those
302 located in the SIV and leading sprouts. Given the semi-circular curvature of the SIVP, ECs in the anterior
303 and posterior of the SIVP migrate shorter distances than ventral ECs in the central region of the plexus.
304 We tracked ECs from 56 hpf onward and analysed their movement between consecutive timepoints,
305 referred to as migration steps.
306
307 ECs near the most ventral sprout were classified as either SIV ECs (blue) or tip cells (magenta) based
308 on their initial position at 56 hpf (Fig. 5A, B), and migration steps were recorded at 30-minute intervals.
309 While the total distance migrated by ECs did not differ significantly between controls and *tnnt2a*
310 morphants (Fig. 5C), the meandering index (total distance/displacement ratio), was significantly
311 reduced in tip cells in *tnnt2a* morphants (Fig. 5D). A meandering index closer to 1, indicates a straighter
312 migration path, while values >1 reflect more tortuous paths. Thus, in the absence of blood flow, tip cells
313 migrated more directly in a ventral direction, with reduced dorsal rearrangement toward the SIV (Fig.
314 5D). In contrast, the meandering index of ECs within the SIV was unaffected by flow status (Fig. 5E).
315 Migration velocity of both tip and SIV ECs gradually decreased in the presence of blood flow, whereas
316 no significant reduction was observed in *tnnt2a* morphants, (Fig. 5F), suggesting that flow may act to
317 slow EC migration and promote vessel stability. Additionally, EC nuclear spacing was reduced in *tnnt2a*
318 morphants (Fig. 5G), consistent with increased EC density in the absence of flow (Fig. 2B").
319
320 We defined migration steps as a relative change in position in both X and Y directions over a 30-minute
321 interval (Fig. 5B). We plotted the overall change in position from their initial starting location at 56 hpf
322 and found that most cells, whether SIV or tip cell, remained within a 5µm radius (Fig.5H, I, K, L). Tip
323 cell migration displayed a larger difference between flow (control morphant) and no-flow (*tnnt2a*
324 morphant) conditions, with control morphants displaying increased dorsal migration (Fig. 5H, J), and
325 *tnnt2a* morphants displaying increased ventral migration (Fig. 5I, J), when compared to each other. Tip

326 cell migration in morphants was more confined along the y-axis (Fig 5H, I, magenta circle), which
327 reflects increased crowding within sprouts (Fig. 5G) and a shift toward ventral rather than dorsal
328 migration (Fig. 5J). Migration steps for SIV cells displayed a markedly reduced difference between
329 conditions (Fig. 5K, L). Most SIV EC migration steps fell within a 5μm radius, with control morphant SIV
330 cells displaying a tendency towards posterior migration (Fig. 5K, M), while *tnnt2a* morphant SIV ECs
331 displayed a significant anterior migration tendency (Fig. 5L, M). This suggests close contact between
332 tip and SIV cells and collective migration of these during SIV development. However, in *tnnt2a*
333 morphants, SIV ECs showed a significant anterior migration bias (Fig. 5K, L, M).
334
335 Together, these data suggest that blood flow provides directional cues for EC migration. During SIVP
336 development, ECs collectively migrate in a ventral-anterior direction as the plexus expands. The onset
337 of flow biases migration; SIV ECs migrate posteriorly, against the direction of flow, while tip cells migrate
338 dorsally, leading to sprout regression and incorporation into the SIV (Fig. 5K). In the presence of flow,
339 SIV ECs shift laterally to accommodate dorsally migrating tip cells as leading sprouts regress. In
340 contrast, without flow, SIV ECs migrate anteriorly, and tip cells migrate ventrally, resulting in elongated
341 sprouts and failed regression. Given that blood flows from posterior to anterior along the SIV (Fig. 1),
342 these findings suggests that flow provides a horizontal mechanical force that guides EC migration
343 during plexus remodelling.
344
345 **Blood flow polarises ECs to initiate reverse migration during sprout regression**
346 During vascular development, ECs polarise in response to migration cues and blood flow (Franco et
347 al., 2015; Kwon et al., 2016). Venous ECs typically exhibit lower levels of polarity compared to arterial
348 ECs (Kwon et al., 2016). To determine whether ECs in the SIVP become polarised in response to flow
349 during sprout regression, we used transgenic zebrafish lines *Tg(fli1a:nls-EGFP)*^{SH549} and *Tg(fli1a:golgi-*
350 *tagRFP, cryaa:CFP)*^{SH529} to label endothelial nuclei and Golgi respectively (Fig. S2A-B). We imaged the
351 SIVP in control and *tnnt2a* morphants at the onset of flow (56hpf) and during sprout regression (64 hpf)
352 quantifying the relative positions of nuclei and Golgi in ECs of leading sprouts and the SIV.
353
354 Prior to flow onset, most tip cells showed ventral Golgi positioning at the migration front with a minority
355 displaying dorsal polarity (Fig. S2B-C). This distribution was not significantly altered in *tnnt2a* morphants
356 (Fig. S2C). Similarly, most SIV ECs were non-polarised before flow began, and no significant
357 differences in polarity were observed between controls and morphants (Fig. S2D). By 64 hpf, once the
358 SIVP was perfused, the proportion of tip cells with dorsally positioned Golgi was significantly reduced
359 in *tnnt2a* morphants. This aligns with our observation that tip cells in morphants undergo persistent
360 ventral migration whereas in controls, they tend to migrate dorsally (Fig. 5J). Additionally, by 64 hpf, a
361 significantly higher proportion of SIV ECs in controls were polarised upstream of flow compared to

362 morphants (Fig. S2B, D). These findings support our cell tracking data (Fig. 5) and suggest that blood
363 flow provides directional cues that coordinate EC and initiate sprout regression.
364
365 To further explore EC rearrangement during sprout regression, we visualised the endothelial actin
366 cytoskeleton using an EC-specific actin nanobody line, *Tg(fli1a:AC-TagRFP)* (Savage et al., 2019) (Fig.
367 S3 & Supplementary Movie 7). Leading sprouts consisted of paired tip cells with their dorsal membranes
368 connected to the SIV lumen (Fig. S3A-D). As regression progressed, both tip cells migrated over each
369 other toward the SIV. The leading tip cell (Fig. S3E-H, green) reoriented its nucleus from a dorsoventral
370 to lateral orientation, with most of its membrane incorporated into the perfused SIV. The adjacent tip
371 cell (Fig. S3I-L, pink) followed, retracting its membrane and re-orienting its nucleus horizontally upon
372 reaching the SIV. Meanwhile the leading tip cell (green) maintained its position, possibly to preserve
373 vessel integrity. During this process, an F-actin positive focus formed at the ventral membrane of the
374 trailing tip cell (Fig. S3H), which developed into a ring-like structure that expanded and eventually closed
375 as the membrane merged with the main vessel (Fig. S3M-P, pink). This suggests dynamic actin
376 reorganisation plays a role in sprout regression. Collectively, these observations indicate that exposure
377 of the dorsal membranes of sprout ECs to blood flow within the SIV lumen is required for plexus
378 remodelling via sprout regression initiation. Furthermore, the coordinated behaviour of neighbouring tip
379 cells appears to ensure sprout regression without compromising vessel integrity.
380

381 **Leading sprout regression occurs under conditions of reduced blood flow**

382 EC rearrangement from regions of low to high shear stress has been implicated in vessel pruning during
383 vascular development (Franco et al., 2015). Shear stress experienced by ECs is directly influenced by
384 haemodynamic flow and blood viscosity, and inversely proportional to the cube of the vessel radius
385 (Heil and Schaper, 2004). Since leading sprouts in the SIVP are not perfused, and tip cells typically
386 regress dorsally in response to SIV perfusion (Fig. 1H-J), we next asked whether reduced blood
387 viscosity is compatible with normal sprout regression. To reduce blood viscosity, we titrated *gata1a*
388 morpholino to deplete circulating erythrocytes by an average of 87% (Fig. 6A-C, arrowheads). Unlike
389 *tnnt2a* loss-of-function (Fig. 2, S1), *gata1a* morphants showed no major changes in overall SIVP
390 morphology (Fig. 6A, B). Interconnecting vessels (ICVs) remained connected to the SIA, and the
391 number of vascular loops was unchanged (Fig. 6D). However, many ICVs were not patent in *gata1a*
392 morphants (Fig. 6B), likely due to reduced erythrocyte flow which may have contributed to the smaller
393 plexus size observed in these larvae (Fig. 6E, F). Surprisingly, the number of leading sprouts was not
394 significantly different between control and *gata1a* morphants (Fig. 6G), indicating that sprout regression
395 can occur under conditions of very low blood flow. In arteries, low shear stress generally induces inward
396 remodelling to increase flow by constricting vessel diameter (Silver and Vita, 2006). These findings

397 support the idea that SIVP remodelling via sprout regression can proceed under low-flow conditions
398 and align with models proposing a low endothelial shear stress set point (Baeyens et al., 2015).
399
400 **Leading sprout regression is dependent on *flt4* under low blood flow conditions**
401 Zebrafish *vegfr4*/*kdrl* and *vegfr2*/*kdr* are individually and co-operatively required for normal SIV
402 formation (Habeck et al., 2002; Koenig et al., 2016). In arteries, sustained deviations from the shear
403 stress set-point trigger vascular remodelling via *flt4* in zebrafish arteries (Baeyens et al., 2015).
404 Additionally, VEGFR1 (Flt1), inhibits excessive venous sprouting in the CNS (Krueger et al., 2011;
405 Matsuoka et al., 2016; Wild et al., 2017) and may act as a decoy receptor to limit angiogenesis
406 (Hiratsuka et al., 1998; Park et al., 1994; Zygmunt et al., 2011). Increased sprouting in the SIVP have
407 previously been reported in *flt1* morphants (Hen et al., 2015), however, the flow status of the SIVP was
408 not examined. We hypothesised that blood flow may regulate *flt1* expression in the SIVP to facilitate
409 regression.
410
411 To test this, we first examined VEGF receptor expression in the SIVP under normal and flow-deficient
412 conditions. Membrane-bound *flt1* (*mflt1*) was undetectable in the SIVP at 56 hpf when sprout regression
413 typically begins (Fig. S4A, B), and at 72 hpf, when regression is complete (Fig S4C, D), regardless of
414 flow status. Similarly, soluble *flt1* (*sflt1*) was not detected in the SIVP at 56 hpf in either condition (Fig.
415 S4E, F). However, at 72 hpf, *sflt1* was present in the SIVP of 40% of *tnnt2a* morphants (Fig. S4G, H,
416 arrow), but absent in controls, suggesting that blood flow may suppress *flt1* expression in the SIVP.
417 This pattern was consistent in the cerebral vasculature where *sflt1* expression was present and
418 unaffected by flow at 56hpf (Fig. S4I, J, arrows), but increased by 72hpf in morphants (Fig. S4K, L,
419 arrows). Since *flt1* was not expressed in the SIVP under normal flow conditions, it is unlikely to be
420 required for sprout regression. Supporting this, sprout regression was normal in *flt1* mutants (Fig. S5A-
421 F) indicating *flt1* is dispensable for this process.
422
423 Kdrl is essential for proper formation and perfusion of the SIVP (Habeck et al., 2002), while Vegfr3/Flt4
424 has been proposed to act as a mechanosensor that regulates the endothelial shear stress set point
425 (Baeyens et al., 2015). Both *kdrl* and *flt4* were broadly expressed throughout the developing SIVP (Fig.
426 S6A-L, arrows) and their expression persisted in leading sprouts which failed to regress in *tnnt2a*
427 morphants (Fig. S6I-L, arrows). *kdrl* expression was unaffected by blood flow status at all examined
428 stages (Fig. S6A, B, E, F, I, J, arrows), whereas *flt4* expression was elevated in the ventral SIVP of
429 *tnnt2a* morphants at 72 hpf compared to controls (Fig. S6K, L, green arrows). In controls, *flt4* expression
430 was reduced during normal sprout regression but remained detectable in non-regressing sprouts in
431 morphants (Fig. S6K, L arrows). Because loss of *kdrl* disrupts SIVP perfusion entirely (Habeck et al.,
432 2002; Koenig et al., 2016) we focused on *flt4* Morpholino knockdown of *flt4* did not impair sprout
433 regression and was compatible with normal remodelling, similar to what we observed with *gata1a*

434 morphants (Fig. S7A-E, arrows). However, simultaneous knockdown of *flt4* and *gata1a* resulted in
435 incomplete sprout regression by 72 hpf compared to controls (Fig. S7D, arrows, E).
436
437 Given known discrepancies between morpholino and mutant phenotypes (Kok et al., 2015), we
438 generated a new *flt4* allele, *flt4*^{qmc316}, using CRISPR mutagenesis This allele contains a frameshift
439 mutation in exon 3 at amino acid 83, resulting in a premature truncation at amino acid 94. The frameshift
440 is caused by a 144 bp insertion and an 8 bp deletion (Fig. S8A).*flt4*^{qmc316} mutants showed no gross
441 morphological defects by 5 dpf (Fig. S8B-C) but lacked a thoracic duct and exhibited impaired
442 craniofacial and meningeal lymphatic formation (Fig. S8D-F), consistent with previously described *flt4*
443 mutants (Hogan et al., 2009b; Shin et al., 2016). Importantly, *flt4*^{qmc316} mutants do not display embryonic
444 oedema up to 5 dpf, allowing us to study the genetic loss of *flt4* without disrupting blood flow in the
445 SIVP. To assess whether *flt4* mutation affects sprout regression, we injected control and titrated *gata1a*
446 morpholinos into embryos from a *flt4*^{qmc316} heterozygous incross. Under normal flow conditions there
447 was no significant difference in leading sprout number between wild-type, heterozygous and mutants
448 (Fig. 7A-D). However, *gata1a* knockdown in *flt4*^{qmc316} significantly increased the number of non-
449 regressing sprouts compared to heterozygous and wild type siblings (Fig. 7E-H). This indicates that *flt4*
450 function is required for effective sprout regression under low flow conditions. These data indicate that
451 while *flt4* is dispensable for sprout regression under normal flow, it is essential for coordinating
452 regression of leading sprouts when flow is reduced. Together, these findings demonstrate that blood
453 flow plays a central role in coordinating endothelial cell migration and sprout regression during vascular
454 plexus formation (Figure 8), establishing a foundation for further exploration of flow-responsive
455 mechanisms in vascular development.
456

457 **Discussion**

458 Developmental remodelling of vascular networks has been described in different models and has mainly
459 focused on pruning of vascular cross branches (Chen et al., 2012; Franco et al., 2015; Kochhan et al.,
460 2013; Lobov et al., 2011; Phng et al., 2009). In this context, pruning occurs in loop forming or cross
461 branch vessel segments, which ultimately leads to regression of the cross branch, leaving behind the
462 two parallel vessels via a process involving EC migration and apoptosis (Chen et al., 2012; Zhang et
463 al., 2018). Dynamic EC migration and rearrangement have also been described in sprouts, however
464 studies have mostly focused on angiogenic sprouting and anastomosis (Arima et al., 2011; Bentley et
465 al., 2014; Jakobsson et al., 2010). Whether sprouts ultimately anastomose with each other, or not, and
466 how these sprouts are remodelled, remained unknown. Here using the zebrafish SIVP we find most
467 leading sprouts within the developing plexus are remodelled via EC migration-driven regression rather
468 than anastomosis. Apoptosis during pruning has been described in murine retinal vessels when
469 circulation is compromised (Franco et al., 2016, 2015; Hughes and Chan-Ling, 2000) and also in
470 zebrafish cranial arteries (Kochhan et al., 2013; Zhang et al., 2018) but this has not been implicated

471 during branch pruning within the SIVP (Lenard et al., 2015). Consistent with this, we tracked
472 approximately 70% of SIVP ECs per plexus and, while we cannot exclude the possibility that EC
473 apoptosis occurs in the most anterior or posterior SIVP, or in the SIA, we observed no apoptotic events
474 following live imaging of over 100 leading sprouts. Therefore, our data suggest that EC migration
475 represents the primary mechanism of sprout regression within the SIVP. Indeed, angiogenic regression
476 is an efficient system because cells are recycled via migration from sprouts, which are temporary
477 structures, to other more permanent structures within developing vessels. Thus, co-ordination of EC
478 migration represents a more efficient use of resources than sculpting vascular networks by proliferation
479 or apoptosis.
480
481 Haemodynamic force exerted by blood flow has been proposed to be crucial in selecting and triggering
482 pruning and regression of particular vessels (Chen et al., 2012; Franco et al., 2015; Kochhan et al.,
483 2013; Lenard et al., 2015; Lucitti et al., 2007). Pruning mostly occurs in small and bifurcated branches
484 with relatively unstable, or low, blood flow in comparison to adjacent large vessels (Chen et al., 2012;
485 Lenard et al., 2015). This observation suggests that pruning is triggered by local differences in flow
486 patterns between branches, which in turn induce EC polarisation and direct EC migration against flow,
487 from low-flow to high flow vessels (Franco et al., 2015). Our data are consistent with this and upon
488 initiation of sprout regression within the SIVP, ECs within the non-perfused leading sprouts are likely
489 'attracted' by the relatively high flow in the SIV, these polarise and migrate out of the regressing sprouts
490 and subsequently contribute to the SIV. In line with this, dorsal-lateral polarisation and migration-
491 induced EC rearrangement are highly dynamic processes during sprout regression and are dependent
492 on blood flow. Interestingly, ventral EC migration persisted throughout the SIVP in *tnnt2a* morphants
493 which indicates a flow-independent mechanism controls this aspect of EC migration. While blood flow
494 co-ordinates remodelling of the SIVP during development, the plexus forms a stereotypical basket-like
495 structure consisting of well-defined branches, SIV and leading sprouts even in the absence of flow. This
496 suggests SIVP formation is regulated by well-orchestrated molecular patterning cues which may
497 interact with physical forces such as blood flow to refine plexus development. Indeed, loss of guidance
498 molecules such as PlexinD1 disrupt SIVP patterning (Goi and Childs, 2016) and PlexinD1 has recently
499 been identified as a shear stress mechanosensor in ECs (Mehta et al., 2020), however, it is unclear
500 whether plexinD1 modulates EC response to flow during SIVP remodelling.
501
502 Remodelling of blood vessels from a primitive structure into a more mature network at onset of flow
503 allows temporal separation of sprouting at the migration front from pruning of branches during
504 angiogenesis (Lenard et al., 2015). In the SIVP, new sprouts are rarely produced after the onset of flow
505 and most existing sprouts remodel via regression. While the entire plexus expands ventrally during this
506 period, the tip cells within leading sprouts do not simply undergo initial ventral migration followed by
507 dorsal migration during regression, rather these ECs display transient and stochastic dorsal migration

508 steps while undergoing collective, flow-independent, ventral migration. This suggests that sprouting and
509 regression are interlinked. An intriguing question is at which point such steps lead to irreversible sprout
510 regression. One possibility is when the tip cells in the sprout come into direct contact with blood flow.
511 At the onset of flow, the posterior membranes of the tip cells are connected with adjacent SIV ECs and
512 have limited exposure to blood flow within the SIV. It is possible that when blood flow creates sufficiently
513 high shear forces on the SIV cells, it drives their migration against flow, and this may exert a pulling
514 force on the tip cells which could promote their dorsal-lateral migration and induce sprout regression,
515 via changes in polarisation. The SIV cells and the tip cells in contact with flow could act as the bridging
516 ECs to sense differences in the local flow environment, as occurs during branch pruning (Franco et al.,
517 2015). That the combined plexus and sprout length in *tnnt2a* morphants was not significantly different
518 to controls indicates that in the absence of blood flow, ECs within sprouts can migrate the same distance
519 as in controls. Reduced plexus length in the absence of blood flow is therefore a consequence of
520 increased contribution of ECs from the branches and SIV to leading sprouts. In the presence of blood
521 flow, ECs within sprouts migrate against flow and contribute to the SIV and branches, thereby
522 supporting their expansion or growth. This is consistent with reports that ECs incorporate in developing
523 arterial networks in the retina and coronary vasculature via coordinated EC migration (Chang et al.,
524 2017; Pitulescu et al., 2017). Our data therefore suggests blood flow promotes regression of leading
525 sprouts within the SIVP as a mechanism to support expansion of the developing plexus. Moreover,
526 sprouting and regression share similar cellular behaviours but in a 'reverse mode'.
527
528 Yolk sac vascular remodelling is dependent upon erythroblast circulation (Lucitti et al., 2007) and
529 uneven erythrocyte distribution in bifurcations has been posited to enhance local shear stress
530 differences between vessels undergoing pruning and their neighbouring vessels (Zhou et al., 2020).
531 Thus, blood viscosity is strongly associated with vessel regression. How ECs sense low levels of flow
532 remains unclear, but several possible molecular mechanisms have been proposed. The level of
533 VEGFR3 has been suggested to maintain a threshold of shear stress sensed by ECs (Baeyens et al.,
534 2015). Interaction of the transforming growth factor β (TGFβ) receptor, activin receptor like kinase
535 ACVRL1/ALK1 with a component of the TGFβ receptor complex, Endoglin, has been reported to
536 enhance EC sensitivity of flow sensing (Baeyens et al., 2016). In addition, non-canonical Wnt signalling
537 may control vessel regression by modulating the threshold for flow-induced EC polarisation (Franco et
538 al., 2016). We find that while plexus length was reduced in erythrocyte depleted embryos, even
539 substantial reductions in blood viscosity were compatible with sprout regression. We find that sprout
540 regression in the SIVP is dependent upon *flt4* under these reduced flow conditions, but *flt4* function is
541 dispensable for sprout regression under normal blood flow. This indicates additional mechanisms could
542 be involved to regulate sprout regression under normal flow conditions. Consistent with this, *flt4* mutants
543 display normal SIVP formation (Hogan et al., 2009a; Hogan et al., 2009b), suggesting different functions

544 of Flt4 under different flow conditions in zebrafish. The established role of VEGFR2 during EC
545 mechanosensation (Coon et al., 2015; Tzima et al., 2005) suggests Kdr and Kdrl are promising
546 candidates to mediate sprout regression under normal flow, however, their requirement during SIVP
547 formation precluded their assessment in this study. The redundant function of Flt4 during sprout
548 regression imparts robustness on the system and facilitates proper vessel remodelling under
549 dysregulated flow conditions. It is important to note that while SIVP leading sprouts are not perfused
550 before or during their regression, a low level of shear provided by skimmed plasma could promote
551 dorsal migration of tip cells to elicit regression (Zhou et al., 2020). Future work will be needed to
552 determine how *flt4* integrates with other mechanosensory pathways and how the mechanosensory input
553 from altered blood flow is transduced by Flt4 to elicit the cytoskeletal changes necessary to rapidly
554 adjust EC migration.
555
556 Together, our data demonstrates that blood flow drives remodelling of a venous plexus by coordinating
557 EC migration and sprout regression and identifies *flt4* as a key mediator under low flow conditions.
558 These insights highlight the dynamic interplay between mechanical forces and molecular signalling in
559 shaping vascular architecture and underscore the importance of flow-responsive pathways in venous
560 remodelling.
561
562

563 **Acknowledgements**

564 We would like to thank the aquarium staff at the University of Sheffield and University of Nottingham
565 for excellent zebrafish husbandry. We thank Freek van Eeden for helpful discussions, Didier Stainier
566 for providing the *flt1* mutant and Katie Fisher for bioinformatic support with cell tracking. This work
567 was supported by a China Scholarship Council and University of Sheffield joint studentship to YC, JG
568 Graves Medical Research Fellowship and Nottingham Research Fellowship to RNW, Diabetes UK
569 (17/0005678 to RNW), BBSRC (BB/R015457/1 to RNW), MRC (MR/X008215/1 to RNW) and British
570 Heart Foundation (RG/19/10/34506 to PCE).
571

572 **Author Contribution**

573 RNW and PCE conceived the project. YC, ZJ, HRK, AMS, PCE, RNW designed experiments; YC, ZJ,
574 HRK, AMS performed experiments, YC, ZJ, AMS, RNW analysed data, RNW and AMS wrote the
575 manuscript and all authors reviewed the final manuscript.
576

577 **Conflicts of Interest**

578 The authors declare no conflicts of interest
579

580 **References**

Akeson A, Herman A, Wiginton D, Greenberg J. 2010. Endothelial cell activation in a VEGF-A gradient: relevance to cell fate decisions. *Microvasc Res* **80**:65–74.

Arima S, Nishiyama K, Ko T, Arima Y, Hakozaki Y, Sugihara K, Koseki H, Uchijima Y, Kurihara Y, Kurihara H. 2011. Angiogenic morphogenesis driven by dynamic and heterogeneous collective endothelial cell movement. *Development* **138**:4763–4776.

Baeyens N, Larrivée B, Ola R, Hayward-Piatkowskyi B, Dubrac A, Huang B, Ross TD, Coon BG, Min E, Tsarfati M, Tong H, Eichmann A, Schwartz MA. 2016. Defective fluid shear stress mechanotransduction mediates hereditary hemorrhagic telangiectasia. *J Cell Biol* **214**:807–816.

Baeyens N, Nicoli S, Coon BG, Ross TD, van den Dries K, Han J, Lauridsen HM, Mejean CO, Eichmann A, Thomas J-L, Humphrey JD, Schwartz MA. 2015. Vascular remodeling is governed by a VEGFR3-dependent fluid shear stress set point. *Elife* **4**.

Bentley K, Franco CA, Philippides A, Blanco R, Dierkes M, Gebala V, Stanchi F, Jones M, Aspalter IM, Cagna G, Weström S, Claesson-Welsh L, Vestweber D, Gerhardt H. 2014. The role of differential VE-cadherin dynamics in cell rearrangement during angiogenesis. *Nat Cell Biol* 1–15.

Bussmann J, Lawson N, Zon L, Schulte-Merker S, Committee, Z. N. 2008. Zebrafish VEGF receptors: a guideline to nomenclature. *PLoS Genet* **4**:e1000064.

Campinho P, Vilfan A, Vermot J. 2020. Blood Flow Forces in Shaping the Vascular System: A Focus on Endothelial Cell Behavior. *Front Physiol* **11**:552.

Chang AH, Raftrey BC, D'Amato G, Surya VN, Poduri A, Chen HI, Goldstone AB, Woo J, Fuller GG, Dunn AR, Red-Horse K. 2017. DACH1 stimulates shear stress-guided endothelial cell migration and coronary artery growth through the CXCL12-CXCR4 signaling axis. *Genes Dev* **31**:1308–1324.

Chen Q, Jiang L, Li C, Hu D, Bu J, Cai D, Jiu-lin. 2012. Haemodynamics-driven developmental pruning of brain vasculature in zebrafish. *PLoS Biol* **10**:e1001374.

Chen Y, Evans PC, Wilkinson RN. 2022. A workflow to track and analyze endothelial migration during vascular development in zebrafish embryos using lightsheet microscopy. *Methods Mol Biol* **2441**:19–28.

Christ B, Poelmann RE, Mentink MM, Gittenberger-de Groot AC. 1990. Vascular endothelial cells migrate centripetally within embryonic arteries. *Anat Embryol* **181**:333–339.

Coon BG, Baeyens N, Han J, Budatha M, Ross TD, Fang JS, Yun S, Thomas J-L, Schwartz MA. 2015. Intramembrane binding of VE-cadherin to VEGFR2 and VEGFR3 assembles the endothelial mechanosensory complex. *J Cell Biol* **208**:975–986.

Ferrara N, Gerber H, LeCouter J. 2003. The biology of VEGF and its receptors. *Nat Med* **9**:669–676.

Fouquet B, Weinstein BM, Serluca FC, Fishman MC. 1997. Vessel patterning in the embryo of the zebrafish: guidance by notochord. *Dev Biol* **183**:37–48.

Franco CA, Jones ML, Bernabeu MO, Geudens I, Mathivet T, Rosa A, Lopes FM, Lima AP, Ragab A, Collins R, Phng L-K, Coveney PV, Gerhardt H. 2015. Dynamic endothelial cell rearrangements drive developmental vessel regression. *PLoS Biol* **13**:e1002125.

Franco CA, Jones ML, Bernabeu MO, Vion A-C, Barbacena P, Fan J, Mathivet T, Fonseca CG, Ragab A, Yamaguchi TP, Coveney PV, Lang RA, Gerhardt H. 2016. Non-canonical Wnt signalling modulates the endothelial shear stress flow sensor in vascular remodelling. *Elife* **5**.

Galloway JL, Wingert RA, Thisse C, Thisse B, Zon LI. 2005. Loss of gata1 but not gata2 converts erythropoiesis to myelopoiesis in zebrafish embryos. *Dev Cell* **8**:109–116.

Goi M, Childs SJ. 2016. Patterning mechanisms of the sub-intestinal venous plexus in zebrafish. *Dev Biol* **409**:114–128.

Habeck H, Odenthal J, Walderich B, Maischein H-M, Schulte-Merker S. 2002. Analysis of a Zebrafish VEGF Receptor Mutant Reveals Specific Disruption of Angiogenesis. *Curr Biol* **12**:1405.

Heil M, Schaper W. 2004. Influence of mechanical, cellular, and molecular factors on collateral artery growth (arteriogenesis). *Circ Res* **95**:449–458.

633 Hen G, Nicenboim J, Mayseless O, Asaf L, Shin M, Busolin G, Hofi R, Almog G, Tiso N, Lawson ND,
634 Yaniv K. 2015. Venous-derived angioblasts generate organ-specific vessels during zebrafish
635 embryonic development. *Development* **142**:4266–4278.
636 Hiratsuka S, Minowa O, Kuno J, Noda T, Shibuya M. 1998. Flt-1 lacking the tyrosine kinase domain is
637 sufficient for normal development and angiogenesis in mice. *Proc Natl Acad Sci U S A*
638 **95**:9349–9354.
639 Hogan B. M., Bos FL, Bussmann J, Witte M, Chi NC, Duckers HJ, Schulte-Merker S. 2009a. Ccbe1 is
640 required for embryonic lymphangiogenesis and venous sprouting. *Nat Genet* **41**:396–398.
641 Hogan Benjamin M., Herpers R, Witte M, Heloterä H, Alitalo K, Duckers H, Schulte-Merker S. 2009b.
642 Vegfc/Flt4 signalling is suppressed by Dll4 in developing zebrafish intersegmental arteries.
643 *Development* **136**:4001–4009.
644 Hughes S, Chan-Ling T. 2000. Roles of endothelial cell migration and apoptosis in vascular
645 remodeling during development of the central nervous system. *Microcirculation* **7**:317–333.
646 Isogai S, Horiguchi M, Weinstein BM. 2001. The vascular anatomy of the developing zebrafish: an
647 atlas of embryonic and early larval development. *Dev Biol* **230**:278–301.
648 Jakobsson L, Franco CA, Bentley K, Collins R, Ponsioen B, Aspalter IM, Rosewell I, Busse M,
649 Thurston G, Alex, Medvinsky A, Medvinsky E, Schulte-Merker S, Gerhardt H. 2010.
650 Endothelial cells dynamically compete for the tip cell position during angiogenic sprouting. *Nat*
651 *Cell Biol* **12**:943–953.
652 Jin S-W, Beis D, Mitchell T, Chen J-N, Stainier D. 2005. Cellular and molecular analyses of vascular
653 tube and lumen formation in zebrafish. *Development* **132**:5199–5209.
654 Kochhan E, Lenard A, Ellertsdottir E, Herwig L, Affolter M, Belting H-G, Siekmann AF. 2013. Blood
655 Flow Changes Coincide with Cellular Rearrangements during Blood Vessel Pruning in
656 Zebrafish Embryos. *PLoS One* **8**:e75060.
657 Koenig AL, Baltrunaite K, Bower NI, Rossi A, Stainier D, Hogan BM, Sumanas S. 2016. Vegfa
658 signaling promotes zebrafish intestinal vasculature development through endothelial cell
659 migration from the posterior cardinal vein. *Dev Biol*.
660 Kok FO, Shin M, Ni C-W, Gupta A, Grosse AS, van Impel A, Kirchmaier BC, Peterson-Maduro J,
661 Kourkoulis G, Male I, DeSantis DF, Sheppard-Tindell S, Ebarasi L, Betsholtz C, Schulte-
662 Merker S, Wolfe SA, Lawson ND. 2015. Reverse Genetic Screening Reveals Poor Correlation
663 between Morpholino-Induced and Mutant Phenotypes in Zebrafish. *Dev Cell* **32**:97–108.
664 Korn C, Augustin HG. 2015. Mechanisms of Vessel Pruning and Regression. *Dev Cell* **34**:5–17.
665 Kroll F, Powell GT, Ghosh M, Gestri G, Antinucci P, Hearn TJ, Tunbak H, Lim S, Dennis HW,
666 Fernandez JM, Whitmore D, Dreosti E, Wilson SW, Hoffman EJ, Rihel J. 2021. A simple and
667 effective F0 knockout method for rapid screening of behaviour and other complex phenotypes.
668 *Elife* **10**. doi:10.7554/eLife.59683
669 Krueger J, Liu D, Scholz K, Zimmer A, Shi Y, Klein C, Siekmann A, Schulte-Merker S, Cudmore M,
670 Ahmed A, Le Noble F. 2011. Flt1 acts as a negative regulator of tip cell formation and
671 branching morphogenesis in the zebrafish embryo. *Development* **138**:2111–2120.
672 Kwan KM, Fujimoto E, Grabher C, Mangum BD, Hardy ME, Campbell DS, Parant JM, Yost HJ, Kanki
673 JP, Chien C. 2007. The Tol2kit: a multisite gateway-based construction kit for Tol2 transposon
674 transgenesis constructs. *Dev Dyn* **236**:3088–3099.
675 Kwon H-B, Wang S, Helker C, Rasouli SJ, Maischein H-M, Offermanns S, Herzog W, Stainier D.
676 2016. In vivo modulation of endothelial polarization by Apelin receptor signalling. *Nat Commun*
677 **7**:11805.
678 Lenard A, Daetwyler S, Betz C, Ellertsdottir E, Belting H-G, Huisken J, Affolter M. 2015. Endothelial
679 Cell Self-fusion during Vascular Pruning. *PLoS Biol* **13**:e1002126.
680 Lobov IB, Cheung E, Wudali R, Cao J, Halasz G, Wei Y, Economides A, Lin HC, Papadopoulos N,
681 Yancopoulos GD, Wiegand SJ. 2011. The Dll4/Notch pathway controls postangiogenic blood
682 vessel remodeling and regression by modulating vasoconstriction and blood flow. *Blood*
683 **117**:6728–6737.
684 Lowe DG. 2004. Distinctive image features from scale-invariant keypoints. *Int J Comput Vis* **60**:91–
685 110.
686 Lucitti JL, Jones EAV, Huang C, Chen J, Fraser SE, Dickinson ME. 2007. Vascular remodeling of the
687 mouse yolk sac requires hemodynamic force. *Development* **134**:3317–3326.

688 Matsuoka RL, Marass M, Avdesh A, Helker CS, Maischein H-M, Grosse AS, Kaur H, Lawson ND,
689 Herzog W, Stainier DY. 2016. Radial glia regulate vascular patterning around the developing
690 spinal cord. *Elife* **5**. doi:10.7554/eLife.20253
691 Mehta V, Pang K-L, Rozbesky D, Nather K, Keen A, Lachowski D, Kong Y, Karia D, Ameismeier M,
692 Huang J, Fang Y, Del Rio Hernandez A, Reader JS, Jones EY, Tzima E. 2020. The guidance
693 receptor plexin D1 is a mechanosensor in endothelial cells. *Nature*. doi:10.1038/s41586-020-
694 1979-4
695 Park JE, Chen HH, Winer J, Houck KA, Ferrara N. 1994. Placenta growth factor. Potentiation of
696 vascular endothelial growth factor bioactivity, in vitro and in vivo, and high affinity binding to
697 Flt-1 but not to Flk-1/KDR. *J Biol Chem* **269**:25646–25654.
698 Phng L, Potente M, Leslie JD, Babbage J, Nyqvist D, Lobov I, Ondr JK, Rao S, Lang RA, Thurston G,
699 Gerhardt H. 2009. Nrarp coordinates endothelial Notch and Wnt signaling to control vessel
700 density in angiogenesis. *Dev Cell* **16**:70–82.
701 Pitulescu ME, Schmidt I, Giaimo BD, Antoine T, Berkenfeld F, Ferrante F, Park H, Ehling M, Biljes D,
702 Rocha SF, Langen UH, Stehling M, Nagasawa T, Ferrara N, Borggrefe T, Adams RH. 2017.
703 Dll4 and Notch signalling couples sprouting angiogenesis and artery formation. *Nat Cell Biol*
704 **19**:915–927.
705 Ribatti D, Crivellato E. 2012. 'Sprouting angiogenesis', a reappraisal. *Dev Biol* **372**:157–165.
706 Savage AM, Kurusamy S, Chen Y, Jiang Z, Chhabria K, MacDonald RB, Kim HR, Wilson HL, van
707 Eeden FJM, Armesilla AL, Chico TJA, Wilkinson RN. 2019. tmem33 is essential for VEGF-
708 mediated endothelial calcium oscillations and angiogenesis. *Nat Commun* **10**:732.
709 Schindelin J, Arganda-Carreras I, Frise E, Kaynig V, Longair M, Pietzsch T, Preibisch S, Rueden C,
710 Saalfeld S, Schmid B, Tinevez J-Y, White DJ, Hartenstein V, Eliceiri K, Tomancak P, Cardona
711 A. 2012. Fiji: an open-source platform for biological-image analysis. *Nat Methods* **9**:676–682.
712 Sehnert AJ, Huq A, Weinstein BM, Walker C, Fishman M, Stainier DYR. 2002. Cardiac troponin T is
713 essential in sarcomere assembly and cardiac contractility. *Nat Genet* **31**:106–110.
714 Shin M, Male I, Beane TJ, Villefranc JA, Kok FO, Zhu LJ, Lawson ND. 2016. Vegfc acts through ERK
715 to induce sprouting and differentiation of trunk lymphatic progenitors. *Development* **143**:3785–
716 3795.
717 Silver AE, Vita JA. 2006. Shear-stress-mediated arterial remodeling in atherosclerosis: too much of a
718 good thing? *Circulation*.
719 Simons M, Gordon E, Claesson-Welsh L. 2016. Mechanisms and regulation of endothelial VEGF
720 receptor signalling. *Nat Rev Mol Cell Biol* **17**:611–625.
721 Thompson MA, Ransom DG, Pratt SJ, MacLennan H, Kieran MW, Detrich HW, Vail B, Huber TL, Paw
722 B, Brownlie A, Oates AC, Fritz A, Gates MA, Amores A, Bahary N, Talbot WS, Her H, Beier
723 DR, Postlethwait JH, Zon LI. 1998. The cloche and spadetail genes differentially affect
724 hematopoiesis and vasculogenesis. *Dev Biol* **197**:248–269.
725 Tinevez J-Y, Perry N, Schindelin J, Hoopes GM, Reynolds GD, Laplantine E, Bednarek SY, Shorte
726 SL, Eliceiri KW. 2017. TrackMate: An open and extensible platform for single-particle tracking.
727 *Methods* **115**:80–90.
728 Tzima E, Irani-Tehrani M, Kiosses WB, Dejana E, Schultz DA, Engelhardt B, Cao G, DeLisser H,
729 Schwartz MA. 2005. A mechanosensory complex that mediates the endothelial cell response
730 to fluid shear stress. *Nature* **437**:426–431.
731 Udan RS, Vadakkan TJ, Dickinson ME. 2013. Dynamic responses of endothelial cells to changes in
732 blood flow during vascular remodeling of the mouse yolk sac. *Development* **140**:4041–4050.
733 Villefranc JA, Amigo J, Lawson ND. 2007. Gateway compatible vectors for analysis of gene function
734 in the zebrafish. *Dev Dyn* **236**:3077–3087.
735 Wild R, Klems A, Takamiya M, Hayashi Y, Strähle U, Ando K, Mochizuki N, van Impel A, Schulte-
736 Merker S, Krueger J, Preau L, le Noble F. 2017. Neuronal sFlt1 and Vegfaa determine venous
737 sprouting and spinal cord vascularization. *Nat Commun* **8**:13991.
738 Wilkinson R, Koudijs MJ, Patient RK, Ingham PW, Schulte-Merker S, Eeden FJ. 2012. Hedgehog
739 signalling via a calcitonin receptor-like receptor can induce arterial differentiation
740 independently of VEGF signalling in zebrafish. *Blood*.
741 Wu RS, Duong DN, Lam II, Clay H, Coughlin SR, Deo RC. 2018. A Rapid Method for Directed Gene
742 Knockout for Screening in G0 Zebrafish. *Dev Cell* **46**:112-125.e4.

743 Zhang Y, Xu B, Chen Q, Yan Y, Du J, Du X. 2018. Apoptosis of Endothelial Cells Contributes to Brain
744 Vessel Pruning of Zebrafish During Development. *Front Mol Neurosci* **11**:222.
745 Zhou Q, Perovic T, Fechner I, Edgar LT, Hoskins PR, Gerhardt H, Krüger T, Bernabeu MO. 2020.
746 Association between erythrocyte dynamics and vessel remodelling in developmental vascular
747 networks. *bioRxiv*. doi:10.1101/2020.05.21.106914
748 Zygmunt T, Gay CM, Blondelle J, Singh MK, Flaherty KM, Means PC, Herwig L, Krudewig A, Belting
749 H, Affolter M, Epstein JA, Torres-Vázquez J. 2011. Semaphorin-PlexinD1 Signaling Limits
750 Angiogenic Potential via the VEGF Decoy Receptor sFlt1. *Dev Cell* **21**:301–314.
751
752

753 **Figures**

754

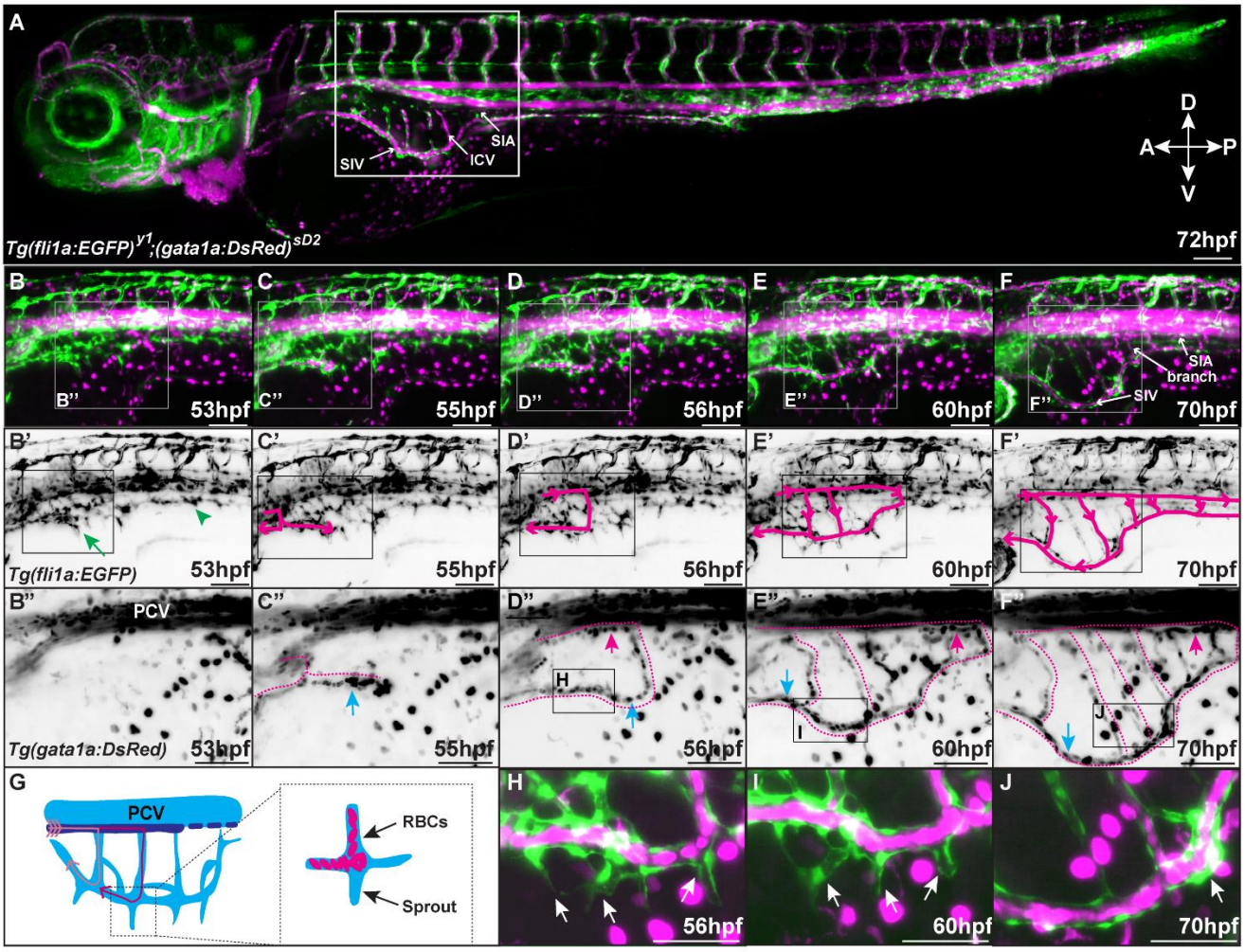

755

756

757 **Figure 1 SIVP perfusion is coincident with leading sprout regression**

758 (**A-F**) Representative images taken from a time-lapse (Supplementary Movie 1) between 53-70hpf
759 showing perfusion of the sub-intestinal venous plexus (SIVP). *Tg(fli1a:EGFP)*^{y1} was used to label
760 endothelial cells (green) and *Tg(gata1a:DsRed)*^{sD2} labels erythrocytes (magenta). Region highlighted
761 in A is displayed in B-F, and region highlighted in B-F is enlarged in B'- F'. Region highlighted in B'-F'
762 is enlarged in B''-F'' and displays the path of circulating erythrocytes. Circulation enters the anterior
763 SIVP between 53hpf (**B-B''**) and 55hpf (**C-C''**) and perfuses the SIV from anterior to posterior as it
764 develops (**D-F''**). Blood enters the SIVP from the supraintestinal artery (SIA) (**D'-F''**, magenta arrows)
765 an extension of the upstream anterior mesenteric artery, through the SIVP branches, drains into the
766 SIV (**C''-F''**, blue arrows) and exits the SIV via the hepatic portal vein (HPV). **G**) Schematic
767 representation of SIVP perfusion. **H-J**) Leading sprouts are observed to regress and undergo
768 anastomosis in the presence of blood flow (arrows). ICV, inter-connecting vessel; PCV, posterior
769 cardinal vein; RBC, red blood cells; SIA, supra-intestinal artery; SIV, sub-intestinal vein. Scale bars =
770 100µm (A-F'), 50µm (B''-J).

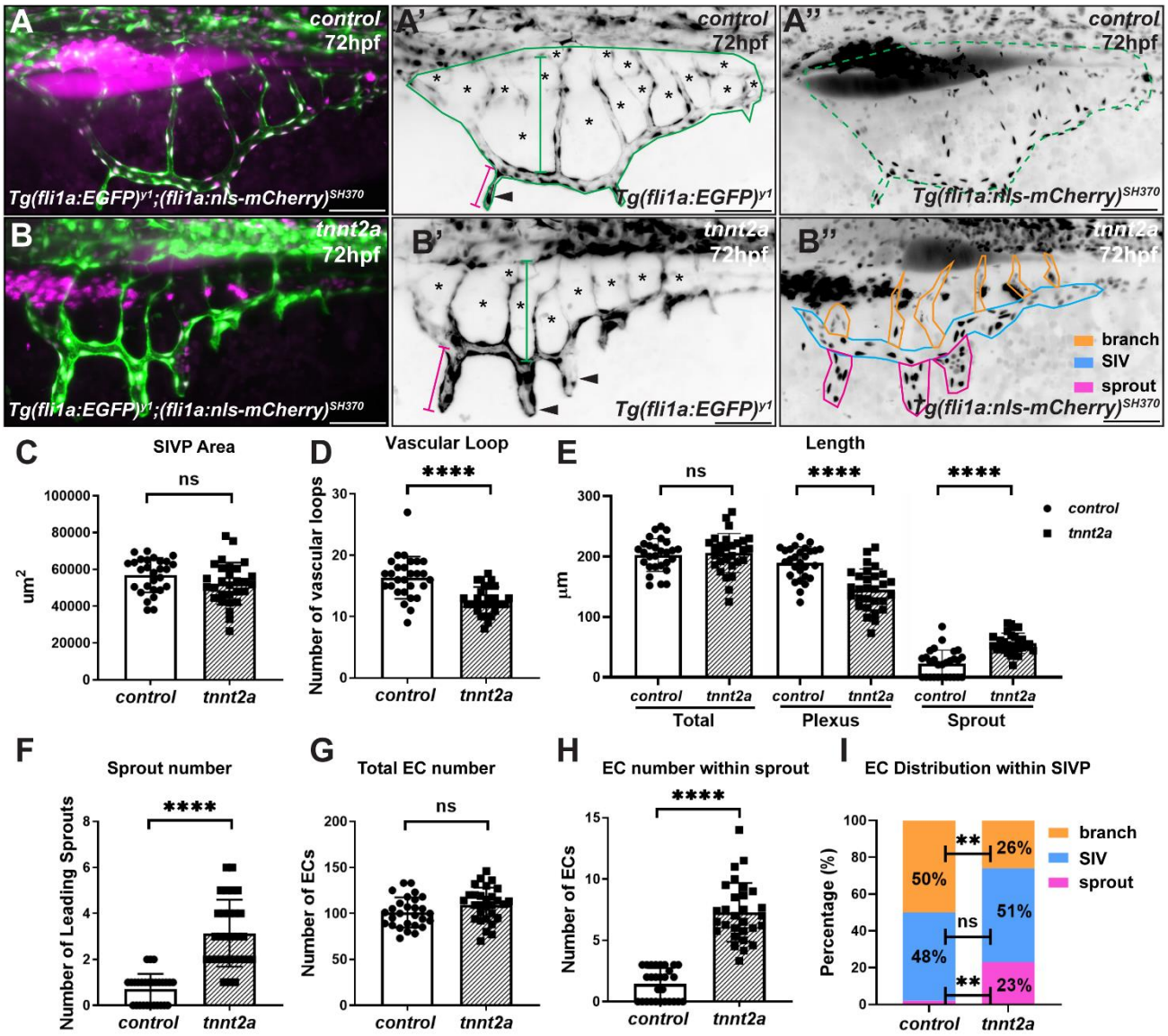

Figure 2 Blood flow controls morphology and endothelial cell distribution of the SIVP

A, **B**) Comparison of SIVP morphology at 72hpf in the presence (control morphants, **A**) or absence of blood flow (*tnnt2a* morphants). **B**) No significant difference in plexus area (highlighted in green in **A'**, **A''**) was observed in the presence or absence of blood flow (**C**). Embryos without blood flow displayed fewer vascular loops (**A'**, asterisks, **D**). Total length of the SIVP plexus was not altered in the presence or absence of blood flow (**B**', green line, **E**), however *tnnt2a* morphant embryos displayed reduced length of the SIVP basket (**B'**, blue line, **E**) and increased sprout length (**B'**, magenta line, **E**). The number of leading sprouts (**A'**, **B'** arrowheads) were increased in *tnnt2a* morphant embryos (**B''**, highlighted in magenta, **F**). The total number of ECs in the SIV was not altered by the flow status of the plexus (**G**), however, leading sprouts contained increased numbers of ECs in *tnnt2a* morphant embryos (**B''**, highlighted in magenta, **H**). In the absence of blood flow, SIV branches contained fewer ECs (**B''**, highlighted in orange, **I**). Unpaired *t*-test, ****$p \leq 0.0001$, ns; $p \geq 0.05$, control embryos, n=28; *tnnt2a* embryos, n=29. Scale bars 50µm.

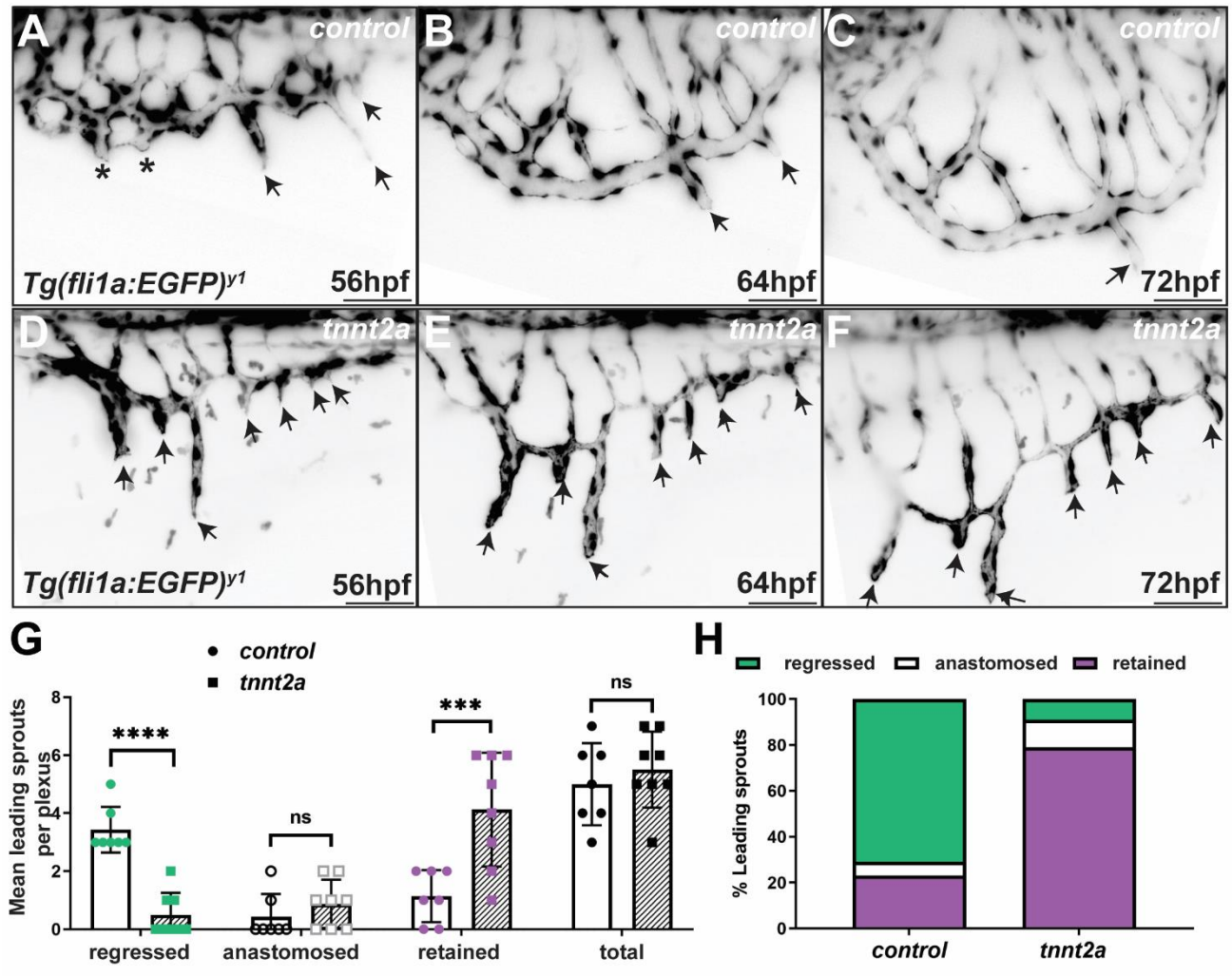

Figure 3 Blood flow promotes regression of SIVP leading sprouts

A-F) SIVP development 56-72hpf in the presence and absence of flow. Still images taken from time lapse movies (Supplementary Movie 3). **A**) In control animals, before blood flow enters the plexus, some angiogenic sprouts from the primary SIV anastomose (asterisks) to form vascular loops, while others lead at the migration front (arrows). **B**, **C**) In controls, leading sprouts regressed following the onset of blood flow and sprout ECs became incorporated into the SIV (arrows). **D-F**) In the absence of flow, leading sprouts failed to regress (**D-F**, arrows). **G, H**) Leading sprout regression was significantly reduced in *tnnt2a* morphant embryos and thus, the number of sprouts present at 72hpf were increased in comparison to controls. Unpaired *t*-test **** $p \leq 0.0001$; *** $p \leq 0.001$; ns $p \geq 0.05$; control morphants n=8; *tnnt2a* morphants n=7. Scale bars 50µm.

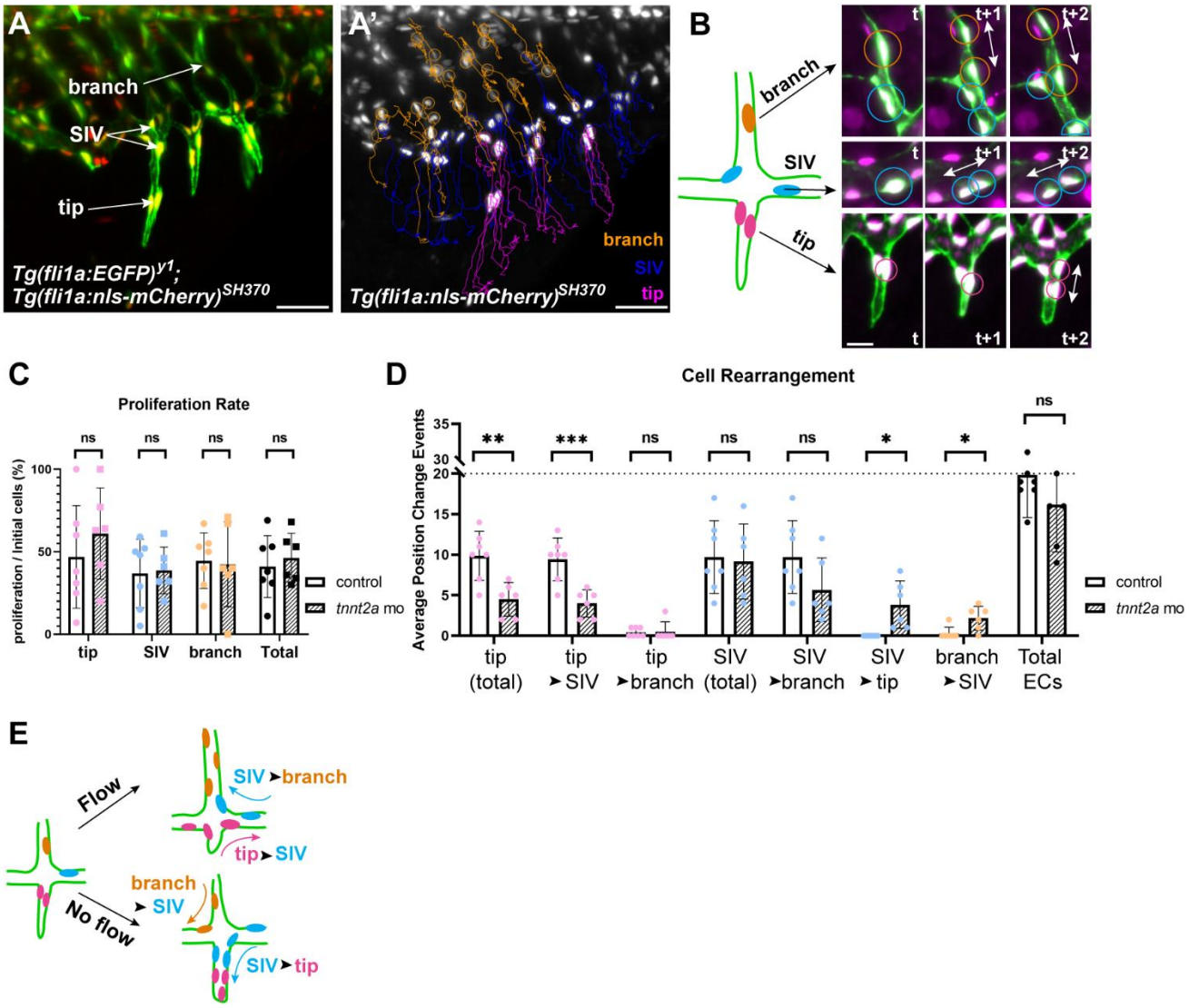

Figure 4 Blood flow coordinates EC migration but not proliferation within the developing SIVP

A-B) ECs in the SIVP were divided into three groups depending upon their initial position at 56hpf. SIVP branch cells (orange) within branches, SIV cells (magenta) within the ventral SIV (blue) and tip cells within leading sprouts (magenta). Examples of EC proliferation in subsequent timepoints are highlighted (**B**). The direction of cell division is parallel to the long axis of the vessel (**B**). **C**) EC proliferation rate (cell division events/initial number of ECs) did not differ in total or between groups in the presence or absence of flow. **D**) There was a substantial reduction in tip cell contribution to SIV in *tnnt2a* morphants, indicating that flow is required for dorsal tip cell rearrangement. In addition, there was an increase in ventral migration of SIV ECs into leading sprouts in the absence of flow. Most branch cells remained in the branches under flow, however, more branch ECs migrated ventrally to contribute to the SIV without blood flow. **E**) Schematic representation of differing EC migration in the presence and absence of blood flow. Unpaired *t*-test ***$p \leq 0.001$; **$p \leq 0.01$; *$p < 0.05$; ns $p \geq 0.05$, control morphants n=7; *tnnt2a* morphants n=6. Scale bars = 50μm (A-A'), 25μm (B).

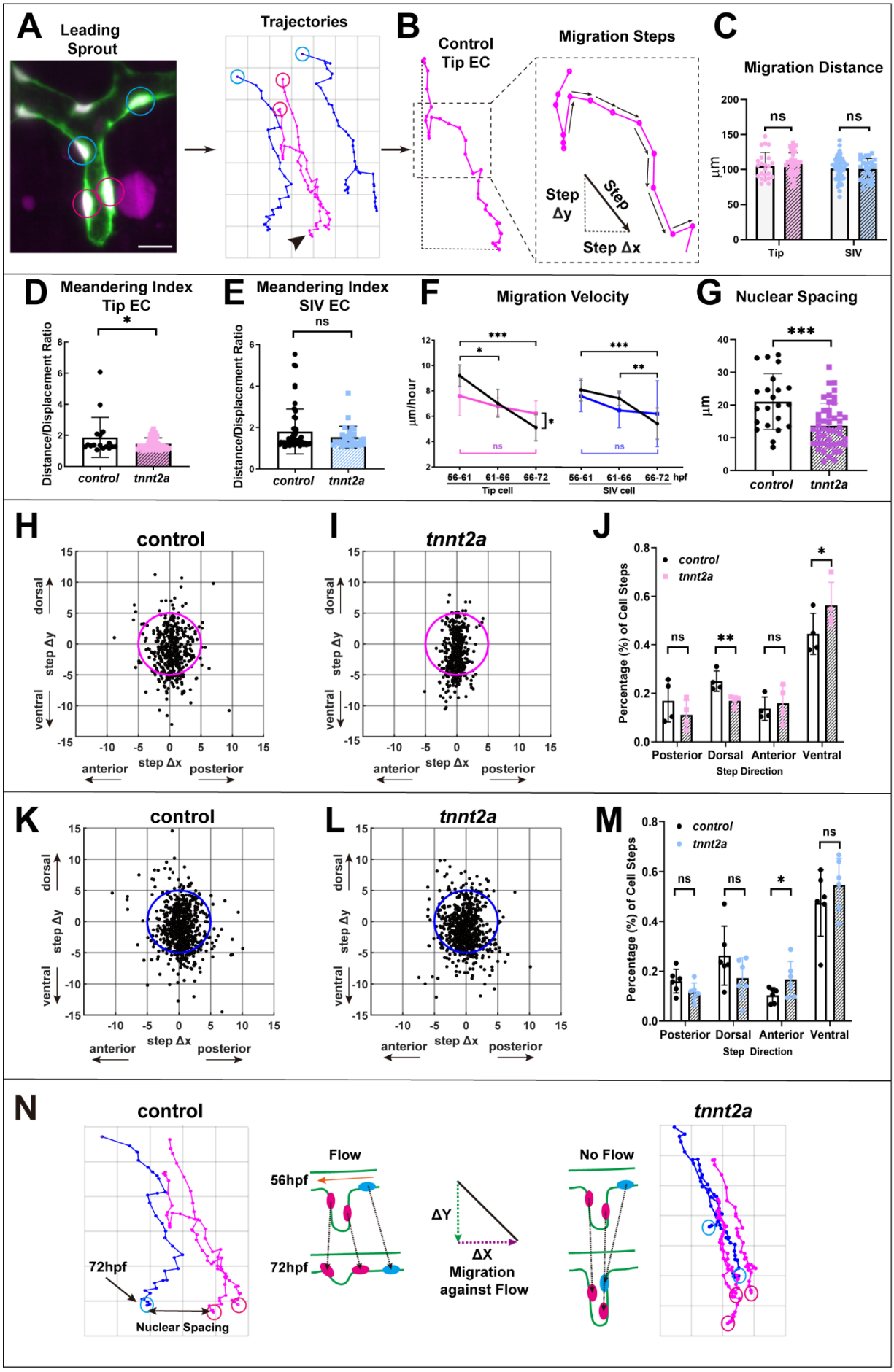
A
Leading Sprout
Trajectories
B
Control Tip EC
Migration Steps
Step Δy
Step
Step Δx
C
Migration Distance
ns
ns
µm
Tip
SIV
D
Meandering Index Tip EC
Distance/Displacement Ratio
control
tnnt2a
E
Meandering Index SIV EC
ns
F
Migration Velocity
µm/hour
56-61
61-66
66-72
Tip cell
SIV cell
hpf
G
Nuclear Spacing
µm
H
control
dorsal
step Δy
ventral
anterior
step Δx
posterior
I
tnnt2a
J
Percentage (%) of Cell Steps
Posterior
Dorsal
Anterior
Ventral
Step Direction
K
L
M
N
Flow
56hpf
72hpf
ΔY
ΔX
Migration against Flow
No Flow
Nuclear Spacing

Figure 5 Blood flow controls EC migration direction during leading sprout regression

A) Examples of ECs within the SIV (blue) or tip cells (magenta) tracked in proximity to leading sprout and example migration trajectories. **B**) Migration 'steps' are defined as the movement of ECs between two consecutive time points (arrows). **C**) Migration distance (the sum of step displacements) of SIV ECs or tip cells was unaffected by flow status of SIVP. (**C-E**) Each dot represents a migration track of a single EC. control, n=79 tracks from 5 embryos; *tnnt2a*, n=64 tracks from 5 embryos. Tip cells: control, n=23 tracks, *tnnt2a*, n=37 tracks; SIV cells, control, n=56 tracks, *tnnt2a*, n=27 tracks; Unpaired *t*-test **D, E**) Meandering index was significantly reduced in tip cells in *tnnt2a* morphants (**D**) but was not significantly different in SIV ECs (**E**). **F**) Migration velocity of tip or SIV cells gradually reduced in the presence of flow (black lines) but was not significantly altered in *tnnt2a* morphants (coloured lines). Average speed of every step of tip cells or SIV cells from 6 control or *tnnt2a* embryos. Unpaired *t*-test. **G**) Nuclear spacing was significantly reduced in *tnnt2a* morphants indicating increased EC crowding within the SIVP. Control, n=22 from 6 embryos; *tnnt2a*, n=46 from 6 embryos. Unpaired *t*-test **H-J**) Scatter plots displaying coordinates of tip cell migration steps. The magenta circle in each plot (5µm radius) is outlined as a reference for coordinate distribution. Migration steps show increased alignment along Y-axis in *tnnt2a* mutants (**I**) in comparison to controls (**H**) and tip cells display significant reduction in dorsal and increase in ventral migration in the absence of blood flow (**J**). control, n=383 steps from 4 embryos; *tnnt2a*, n=860 steps from 4 embryos. **K-M**) Scatter plots displaying coordinates of SIV EC migration steps indicate increased migration steps in quadrant III in *tnnt2a* morphants (**L**) indicating anterior migration bias in the absence of blood flow (**M**). control, n=1313 steps from 6 embryos; *tnnt2a*, n=744 steps from 6 embryos. **N**) Schematic representation of EC migration within the SIVP during sprout regression. In the presence of flow, SIV cells migrate laterally to accommodate dorsally migrating tip cells as leading sprouts regress. In the absence of flow, SIV ECs migrate more anteriorly, and tip cells migrate ventrally leading to elongated sprouts and regression failure. **** $p \leqslant 0.0001$; *** $p \leqslant 0.001$; ** $p \leqslant 0.01$; * $p < 0.05$; ns $p \geq 0.05$. Scale bar 25µm.

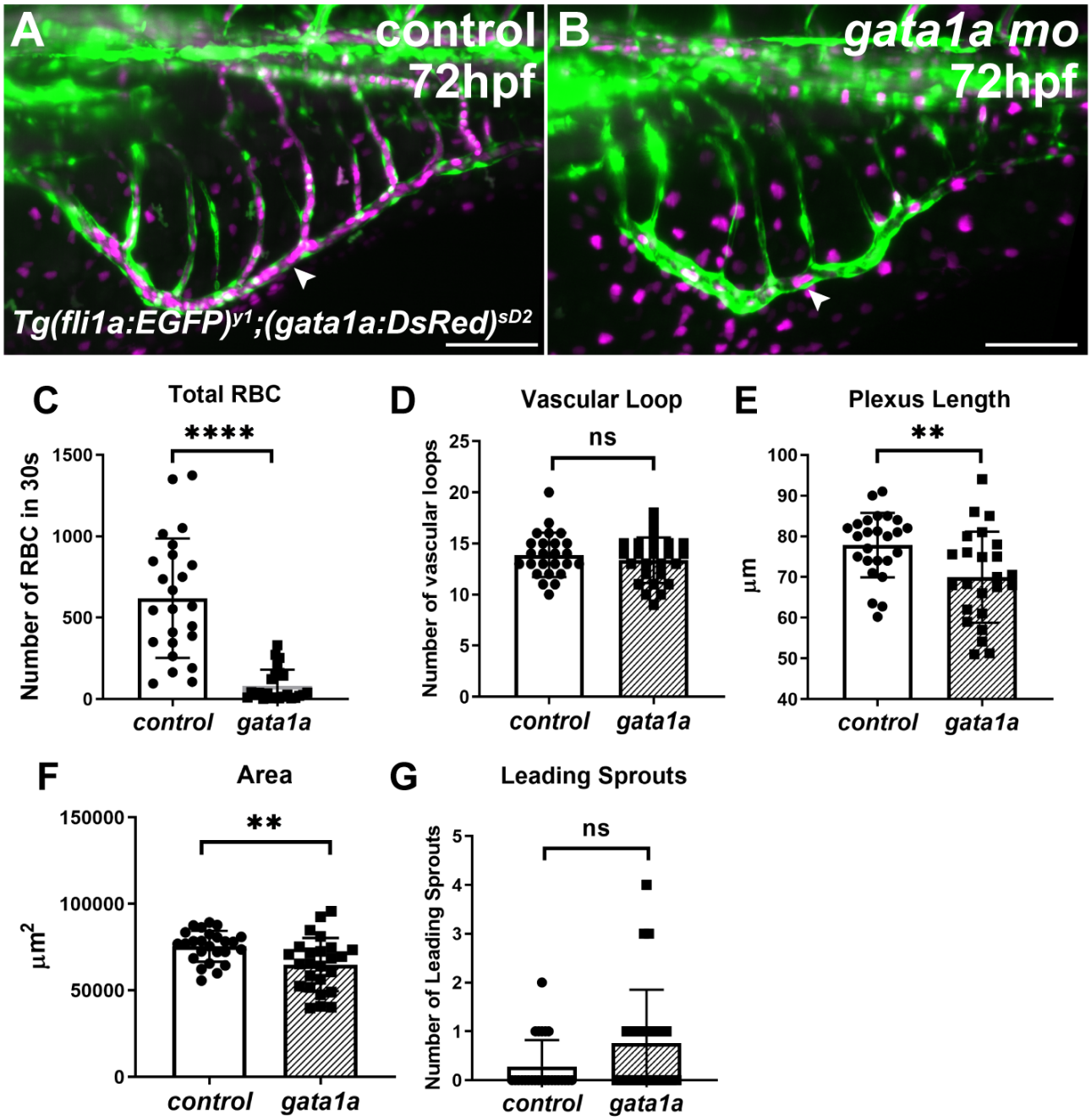

Figure 6 Leading sprout regression occurs under conditions of reduced blood flow

Leading sprouts undergo normal regression in *gata1a* morphants (**A**) in comparison to controls (**B**) despite a substantial reduction of circulating erythrocytes in *gata1a* morphants (**C**). Frequency of vascular loops did not differ between *gata1a* morphants and controls (**D**), but plexus length (**E**) and area (**F**) was reduced in *gata1a* morphants. Frequency of leading sprouts was not significantly altered in *gata1a* morphants (**G**). Unpaired *t*-test, **** $p \leq 0.0001$; ** $p \leq 0.01$; * $p < 0.05$; ns $p \geq 0.05$; control morphants n=24, *gata1a* morphants n=24, 3 replicates. Scale bars 50µm.

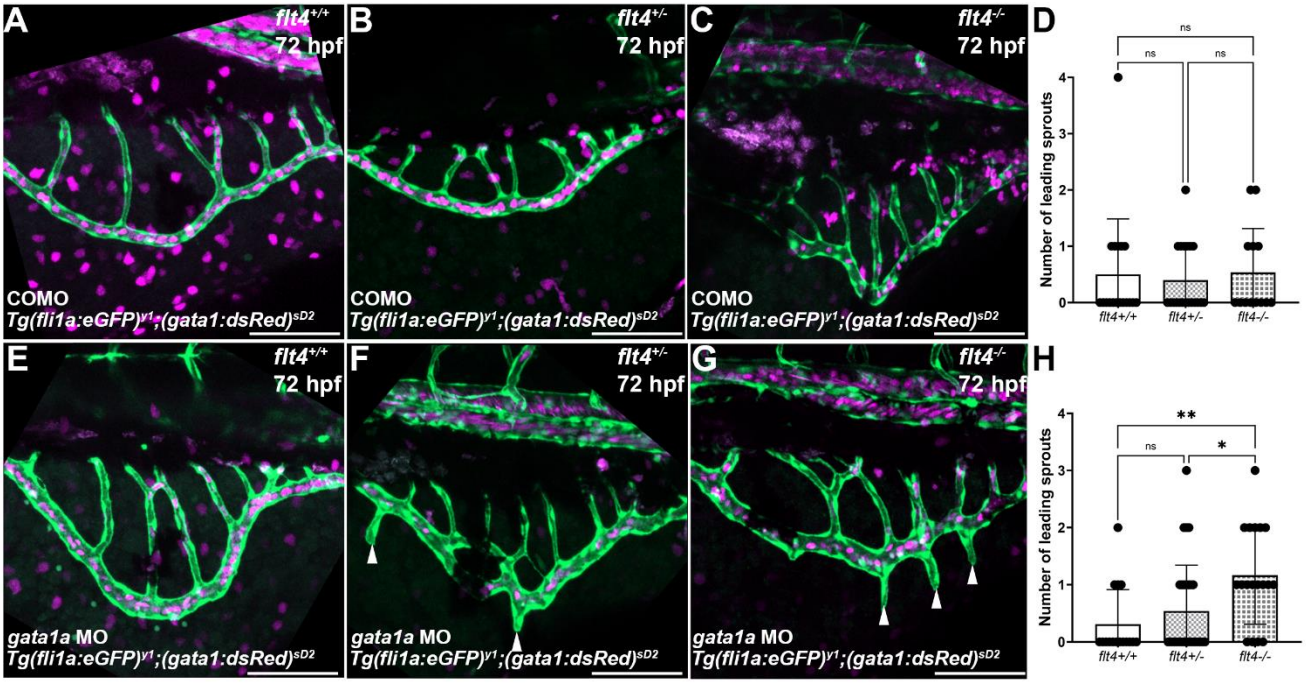

Figure 7 Leading sprout regression under low blood flow conditions is dependent on *flt4*

The number of leading sprouts observed in wild type (**A**), *flt4* heterozygous mutants (**B**), or *flt4* homozygous mutants (**C**) under normal flow conditions, injected with morpholino, was not significantly different (**D**). Low flow conditions, caused by *gata1* morpholino injection did not increase leading sprout numbers in wild type (**E)** or *flt4* heterozygous mutants (**F**), but leading sprouts in *flt4* homozygous mutants (**G**; white arrowheads) were significantly increased in number (**H**). One-way ANOVA, ** $p \leqslant 0.01$; * $p \leqslant 0.05$; ns $p \geq 0.05$. control morphant *flt4*$^{+/+}$ n=18; control morphant *flt4*$^{+-+}$ n=20; control morphant *flt4*$^{-/-+}$ n=13; gata1 morphant *flt4*$^{+/+}$ n=16; gata1 morphant *flt4*$^{+-+}$ n=37; gata1 morphant *flt4*$^{-/-}$ n=18, 3 replicates each. Scale bars 100µm.

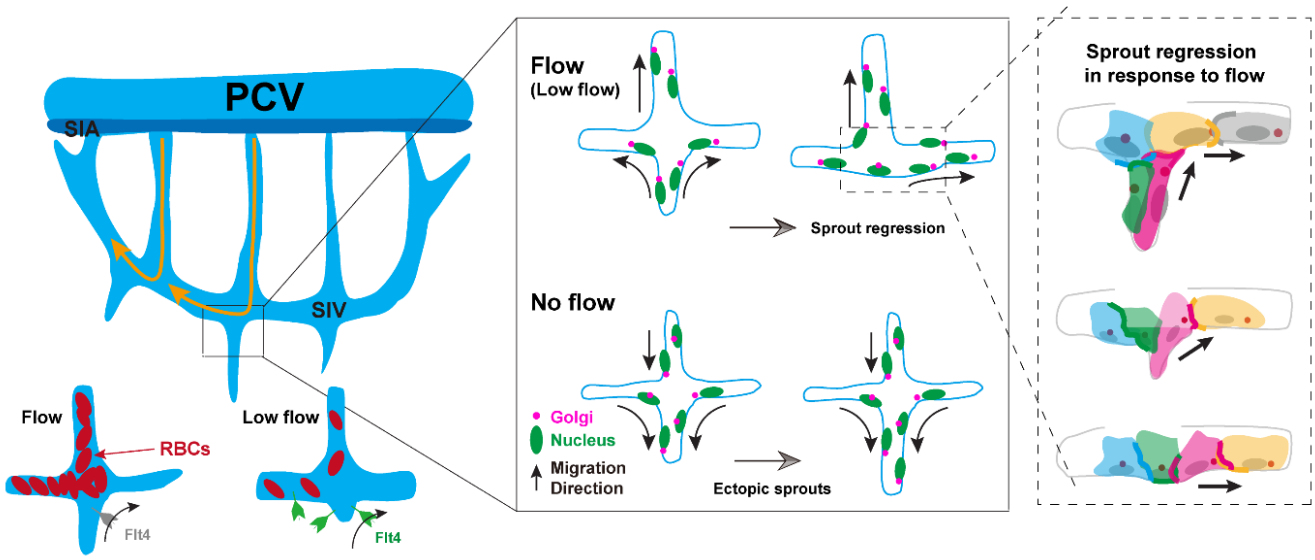

Figure 8 Cellular mechanisms of flow-mediated sprout regression

Schematic illustrations depicting the cellular behaviours during SIVP sprout regression in the presence and absence of flow. Blood flow promotes EC Golgi polarisation, dorsal and lateral EC migration and leads to sprout regression via Flt4 under low blood flow conditions. Illustrations highlighted with dashed lines depict co-ordination of EC migration during sprout regression in response to flow. ECs (in grey and yellow) at the luminal surface migrate laterally against flow and ECs (in green and pink) in the regressing sprout are pulled or use their neighbouring cells as migratory substrates via EC junctions (thickened lines), followed by EC rearrangements which lead to sprout regression. Abbreviations; PCV posterior cardinal vein; RBCs, red blood cells; SIV; sub-intestinal vein; SIA, supra-intestinal artery